JACS
JOURNAL OF THE AMERICAN CHEMICAL SOCIETY
pubs.acs.org/JACS
Article

Crystallization of Cholesterol in Phospholipid Membranes Follows Ostwald's Rule of Stages

Soohyun Park, Tun Naw Sut, Gamaliel Junren Ma, Atul N. Parikh, and Nam-Joon Cho*

Cite This: https://dx.doi.org/10.1021/jacs.0c10674
Read Online

ABSTRACT: Crystallization of membrane-embedded components within phospholipid bilayers represents a distinct class of phase transformation that occurs in structurally organized, molecularly crowded, and dimensionally constrained amphiphilic fluids. Using unstable supported lipid bilayers—transiently assembled via surface-mediated fusion and spreading of bicellar precursors containing supersaturating concentrations of cholesterol—we monitor here the morphological evolution and dynamics of cholesterol crystallization within the membrane media. We find that the three-dimensional (3D) crystallization of cholesterol from an unstable two-dimensional (2D) in-membrane state proceeds via well-defined sequence of intermediates, including filaments, rods, helices, and 2D rectangular plates, before transforming into three-dimensional quadrilateral crystals—characteristic triclinic habit of cholesterol monohydrate. Our observations thus demonstrate that these structurally distinct cholesterol polymorphs are related to one another, contrasting with the notion that they represent disparate crystal habits stabilized by differences in lipid environments. Moreover, these observations indicate that cholesterol crystallization within the membrane media follows nonclassical multistep crystallization governed by the heuristic "Ostwald's rule of stages", which predicts that the crystallization kinetics proceed down the free energy landscape in a multistage process where each successive phase transition incurs the smallest loss of free energy relative to its predecessor. Furthermore, we find that the well-known cholesterol extracting agent, β-cyclodextrin, acts by catalytically tipping the equilibrium in favor of crystal growth adding cholesterol from the membrane phase to the crystal in a layer-by-layer manner. Taken together, our results provide a new description of in-membrane cholesterol crystallization and may pave for a screening tool for identifying molecular candidates that target cholesterol crystals.

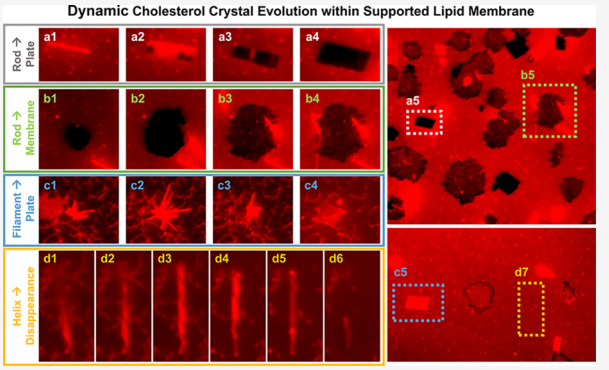

INTRODUCTION

When a thermodynamically stable system is quenched, such as by a sudden and drastic change of external conditions, it falls out of thermodynamic equilibrium and enters an unstable state. The subsequent relaxation of this nonequilibrium system—in which the "old" mother phase evolves toward a new equilibrium phase—is often complicated. The kinetics are especially exacerbated when a phase boundary is crossed and more than one phase is locally stable. Depending on the complexity of the energy landscape, the trajectory of the crystallizing (or phase separating) component(s) deviates nontrivially from the predictions of classical nucleation and growth based model of crystallization.[1] Here, the phase ordering processes[2] characterizing the crystallization pathway from an unstable state do not directly produce the thermodynamically most stable state, but rather transient metastable intermediates first appear. This scenario was first conjectured by Ostwald as early as 1897.[3] In his empirical "rule of stages", Ostwald suggested that the phase transformation proceeds down the free energy landscape in a multistage, staircase cascade—where each successive phase transition incurs the smallest loss of free energy relative to its predecessor—accessing available metastable polymorphs before reaching the stable ground state. Although exceptions exist, this simple heuristic principle has since been shown to qualitatively explain phase ordering dynamics across many disparate systems. Some examples include the formation of long-lived metastable intermediates during bulk crystallization of proteins,[4] colloids,[5,6] and broad classes of inorganic materials.[7−9]

The considerations above are of great interest in a variety of soft matter and biological systems where phase transformations occur in dimensionally constrained, structurally organized, and molecularly crowded environments. This is perhaps best

Received: October 8, 2020

https://dx.doi.org/10.1021/jacs.0c10674
J. Am. Chem. Soc. XXXX, XXX, XXX−XXX

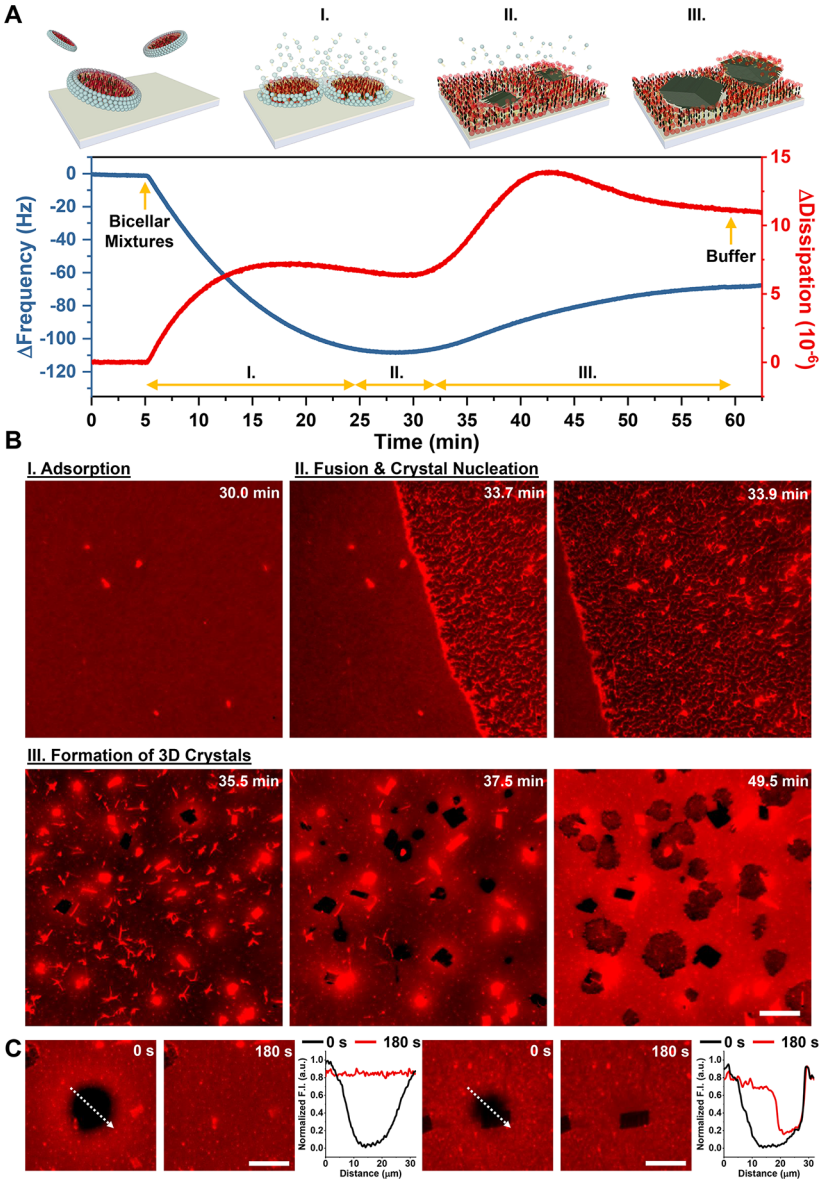

Figure 1. Observation of the supported lipid membrane formation from cholesterol-rich bicellar mixtures via QCM-D and fluorescence microscopy. (A) QCM-D measurements of adsorption of bicellar mixtures are presented for changes in overtone 7th frequency (Δf) and energy dissipation (ΔD) as a function of time. Baseline signals in equivalent buffer solution were recorded before injecting bicellar mixtures at 5 min. (B) Microscopic observation of the supported lipid membrane formation on a glass surface for bicellar mixtures (with 0.5 mol % of labeled long-chain lipid, Rh-PE). Image snapshots at various time points demonstrate the following steps: (I) adsorption of bicellar mixtures, (II) fusion or rupture of adsorbed bicellar mixtures and cholesterol crystal nucleation, and (III) formation of 3D crystals. t = 0 min corresponds to the time when the addition of bicellar mixtures was begun. (C) Fluorescence recovery after photobleaching (FRAP) analysis was performed to characterize fluidic cholesterol-enriched supported lipid membranes. The photobleaching was performed at t = 0 s, and the bleached spot corresponds to the dark spot in the center of the micrograph. The normalized fluorescence intensity (F.I.) as a function of distance across the bleached area (white dotted arrow in 0 s images) is presented in corresponding cases. The F.I. was normalized by setting minimum and maximum F.I. values throughout the time as 0.0 and 1.0 au, respectively. The mobile fraction (mobile %) was calculated by recovery curve obtained from the full circular bleached region (see Figure S2). The scale bars are 20 μm.

exemplified by phase changes that take place within cellular membranes. Examples include lateral phase separation of membrane components[10,11] and crystallization of cholesterol, a membrane amphiphile;[12] membrane proteins,[13] such as bacteriorhodopsin; membrane-associated proteins,[14,15] such as bacterial and archaeal S layer proteins; and even membrane pores lined by antimicrobial peptides.[16] In all of these cases, the energy landscape, which the phase-separating or crystallizing species traverses, is rendered complex by the reduced dimensionality, composition-dependent elastic behaviors, and diffusional complexities of the host membrane, allowing for a host of metastable intermediates.

Within this general context, the case of cholesterol crystallization within the membrane environment represents a distinct class. From a fundamental point of view, three-dimensional crystallization of the native membrane amphiphile from a quasi-two-dimensional membrane is interesting because it involves a complicated interplay with membrane lipids, with which cholesterol has preferential interactions. Furthermore, *in-membrane* cholesterol crystallization is important not only

https://dx.doi.org/10.1021/jacs.0c10674
J. Am. Chem. Soc. XXXX, XXX, XXX−XXX

because of its ubiquity in mammalian membranes but also because of its pathological relevance. Although cholesterol concentration in mammalian membranes is strictly regulated, dysfunction in cholesterol homeostasis, leading to abnormal levels of cholesterol concentrations, is not uncommon. It is responsible for many diseased states where concentrations of cholesterol exceed the solubility limit in the lipid bilayer environments of cellular membranes;[17] the same occurs in micellar/vesicular environment of bile salts. Under these conditions, clusters of cholesterol "precipitate" from their homeostatic membrane environment, forming discrete, three-dimensional (3D) cholesterol crystals. Indeed, cholesterol crystals have been observed in atherosclerotic tissues, cell cultures, and micellar/vesicular bile salts and have been shown to be associated with the corresponding pathological conditions including atherosclerosis,[18,19] gallstones,[20,21] and age-related macular degeneration.[22] In most of these cases, cholesterol crystallizes as a monohydrate in one of two primary habits: (1) triclinic, which is energetically most stable and appears as quadrilateral plates, and (2) the less stable monoclinic habit, which is characterized by rodlike elongated morphologies.

Studies using experimental models of membranes—including those utilizing monolayers, single supported bilayers, and multilayers of predetermined cholesterol−phospholipid mixtures—have proved remarkably valuable in deciphering the nuances of cholesterol crystallization pathways. Collectively, these studies show that cholesterol segregates[23−26] in a single lipid bilayer environment producing 2D rectangular domains, which "epitaxially" seed the formation of 3D crystals.[26−28] These studies also reveal that the 2D-to-3D dimensional transformation of cholesterol crystals depends strongly on the lipid composition: some compositions favor direct nucleation of triclinic polymorph[28,29] whereas others produce coexisting populations of both monoclinic and triclinic polymorphs.[28,30]

Despite the progress these and other related studies portend, our understanding of the kinetic pathways by which cholesterol crystallize within the membrane media remains incompletely understood. Do thermodynamically less stable, monoclinic cholesterol monohydrate crystals appear as metastable intermediates en route to the formation of triclinic quadrilateral plates as would be predicted by Ostwald's rule of stages? If yes, what are their lifetimes? Can 2D precursor bilayers transiently accumulate sufficient cholesterol to become unstable and prompt 3D crystallization? If not, does the growth of 3D cholesterol crystals require exogenous supply of cholesterol? How is the lipid environment perturbed during and upon cholesterol crystallization? Experimentally addressing these questions has remained challenging because they require preparation of model membrane configurations that are supersaturated with cholesterol and thus unstable.

In the work reported here, we take steps in elucidating the pathways of cholesterol crystallization within unstable lipid bilayers containing supersaturating concentrations of cholesterol. We demonstrate that the requisite unstable membrane configurations containing cholesterol at supersaturating concentrations can be transiently produced using cholesterol-laden bicellar precursors and that their relaxation pathways, involving cholesterol crystallization, can be monitored *in situ*. Using real-time epifluorescence microscopy, we show that a surface adsorption of bicellar mixtures, containing high levels of cholesterol, enable a formation of contiguous bilayers, which spontaneously relax over experimentally accessible time scales producing three-dimensional cholesterol crystals. Documenting these dynamics, we capture a temporal appearance of short-lived helical monoclinic intermediates, en route to the formation of familiar quadrilateral plates of the triclinic polymorph. This then lends direct support for the hypothesis that cholesterol crystallization in membrane-like lipid bilayer environment is indeed governed by Ostwald's rule of stages. In addition, considering the clinical significance of dysfunction in cholesterol homeostasis, we further provide a proof-of-principle suggesting the suitability of cholesterol-rich supported membranes for screening drug candidates that target cholesterol crystals.

RESULTS AND DISCUSSION

We begin by investigating the transient formation of the supported lipid bilayers containing saturating levels of cholesterol from their bicellar precursors (see the Experimental Section). It is now well established that phospholipid bicelles adsorb, fuse, and rupture onto silica surfaces to form supported lipid bilayers (SLBs).[33−36] To test whether these approaches can be extended to supersaturated cholesterol-laden bicellar mixtures, we used quartz crystal microbalance with dissipation (QCM-D) measurements. These measurements track the mass and viscoelastic properties of the adsorbing layer in real time by recording changes in the resonance frequency (Δf) and the energy dissipation (ΔD), respectively. After the baseline stabilization in equivalent buffer solution (∼5 min), we injected bicellar mixtures for ∼50 min and recorded Δf and ΔD as a function of incubation time (Figure 1A). Time traces of Δf and ΔD reveals three discernible regimes of bicelle−surface interactions. The first regime (step I), which commences immediately after the initial stabilization (∼5−25 min), is characterized by a sharp decrease in the resonant frequency (negative Δf) and a corresponding increase in the energy dissipation (positive ΔD). The former indicates mass increase consistent with the expected adsorption of bicellar mixtures at the surface, and the latter confirms that the resulting adsorbed layer is not rigid.

This regime is followed by a short-lived second regime (step II, ∼25−30 min) where the asymptotic frequency response reveals a slight upward trend and that of dissipation reveals a small, but measurable, decrease. These observations are consistent with the fusion and rupture of the adsorbed bicellar mixtures at the surface. In step III, both Δf and ΔD begin to increase, suggesting continued molecular rearrangements. Although the positive Δf values generally imply the loss of adsorbed mass (e.g., when adsorbed vesicles rupture and form SLBs), they can also reflect adsorption in thick viscoelastic layers.[37−39] Thus, the observed increase of both Δf and ΔD in step III suggests the formation of three-dimensional crystals within the adsorbed layer, which can be seen from the mass uptake perpendicular to the shearing surface direction during the three-dimensional crystal growth.[40] Visualizing the label-free samples used in QCM-D using bright-field microscopy reveals multiple, geometrically distinct populations of substructures including quadrilateral plates and rodlike crystal domains (Figure S1).

To gain real-time insight into the appearance, transformations, and dissolution of the substructures that form during equilibration of lipid bilayers containing supersaturating cholesterol concentrations, we probe real-time structural evolution of the transient supported membranes produced by bicelle−surface interactions using fluorescence microscopy.

https://dx.doi.org/10.1021/jacs.0c10674
J. Am. Chem. Soc. XXXX, XXX, XXX−XXX

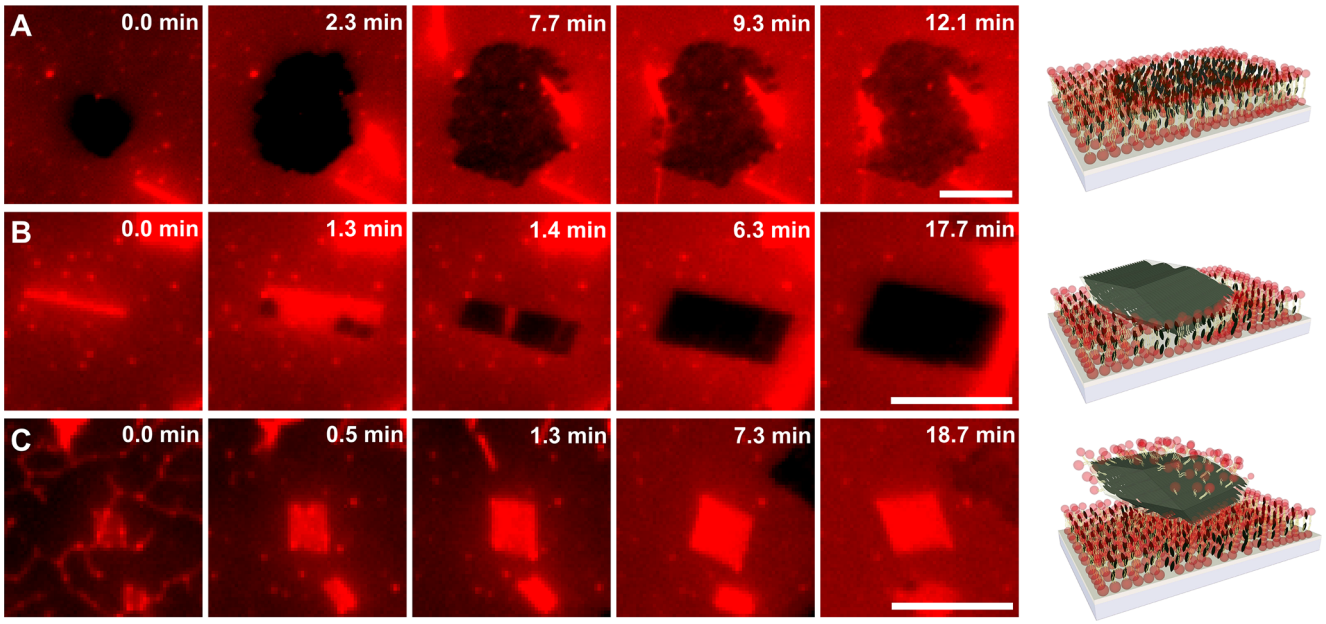

Figure 2. Microscopic observation of the dynamic cholesterol crystal evolution after supported lipid membrane formation from supersaturated cholesterol-laden bicellar mixtures. Microscopic observation of the dynamic cholesterol crystal growth from cholesterol bicellar mixtures. The formation of (A) rods dissolving into cholesterol-enriched domains at the membrane surface, (B) rods converting into quadrilateral plates, and (C) evolution toward the equilibrium triclinic polymorph covered by lipids were captured during the time-lapse imaging. In each case, the first image was set to 0 min to follow the timeline of evolution, and the scale bars are 10 μm.

The visualization by fluorescence is enabled by simply doping the bicelle lipid mixture with 0.5 mol % 1,2-dioleoyl-*sn*-glycero-3-phosphoethanolamine-*N*-(lissamine rhodamine B sulfonyl) (ammonium salt) (Rh-PE). These fluorescently labeled bicellar mixtures are then introduced using a microfluidic chamber under a flow-through condition, and time-lapse images of the resulting surface structures were captured.

During the first 30 min, the fluorescence intensity at the silica surface gradually increases, culminating into a uniform fluorescence (at the optical scale) with a sparse concentration of brighter aggregates scattered across the macroscopic surface. This surface accrual of fluorescence is entirely consistent with the stochastic adsorption of the bicellar mixtures at silica (Figure 1B, step I), leading to a saturating surface coverage. At about 30 min, a sudden dramatic change, lasting ~30 s, sweeps through the observed field of view (step II). Here, the uniform fluorescence is abruptly replaced by a dense network of fluorescent fibrils. We ascribe this dramatic change to signal interbicelle fusion (step II), transiently producing a contiguous supported lipid bilayer. Because cholesterol concentration in the resulting bilayers exceeds its solubility, the bilayer is expected to be unstable to the lamellar morphology consistent with the observed transition from the lamellar to the fibrillar state. (Note that the QCM-D measurement is ensemble-averaged; thus, step II observed from the signal is much longer (~5 min) than the one from fluorescence microscopy imaging.)

Over the course of the next ~20 min, this fibrillar pattern undergoes another radical transformation replacing the initial network by a rapidly evolving and highly dynamic surface structure. This elaborate surface patterning occurs spontaneously and produces concurrently a dynamic mosaic of populations of geometrically distinct substructures, both fluorescent and nonfluorescent, which appear, grow, translate, and dissolve (Movie S1). In what follows, we describe major features of this structural evolution.

We begin by asking whether the lipid bilayer itself—in the face of such large-scale structural remodeling—retains its long-range structural integrity. To address this question, we monitored the lateral diffusion of fluorescently labeled lipids (Rh-PE) within the lipid phase using a microscopy-based fluorescence recovery after photobleaching (FRAP) measurement (Figure 1C). We photobleached large, tens of micrometers wide, circular spots in both the lipid-rich regions away from the crystals and the immediate proximity of rectangular plates. In both cases, we find near-complete recovery of large microscopic photobleached spots within 3 min with ~90% mobile fraction, confirming the large-scale fluidity and contiguity of the lipid bilayer phase. Moreover, quantifying the fluorescence recovery profiles yields the lateral diffusivity of 2.5 $\mu m^2/s$, in good agreement with those reported previously for well-formed supported lipid bilayers.[33] A detailed analysis of FRAP is given in Figure S2. These observations also lend additional support to our foregoing inference that the initial bicellar mixtures, upon surface adsorption, fuse and produce a contiguous lipid bilayer.

A closer inspection of the temporal sequence of fluorescence images sheds light on the pathway characterizing cholesterol crystallization during this regime (step III); these are discussed in turn below. The dense network of phospholipid-covered flexible fibrils we observe at the onset of bilayer evolution marks the first step. The fibrils are interconnected with tens of micrometers long along their long-axis and have diameters 0.5−1 μm, close to the optical resolution in our experiments. They are fluorescently bright, indicating that they are lipid-laden. This network of fibrils is rather short-lived. Seconds after their appearance, neighboring fibrils appear to coalesce, transforming into wider rods, tens of micrometers in length. They exhibit elevated fluorescence [F.I.(rod)/F.I.(thread) =

https://dx.doi.org/10.1021/jacs.0c10674
J. Am. Chem. Soc. XXXX, XXX, XXX−XXX

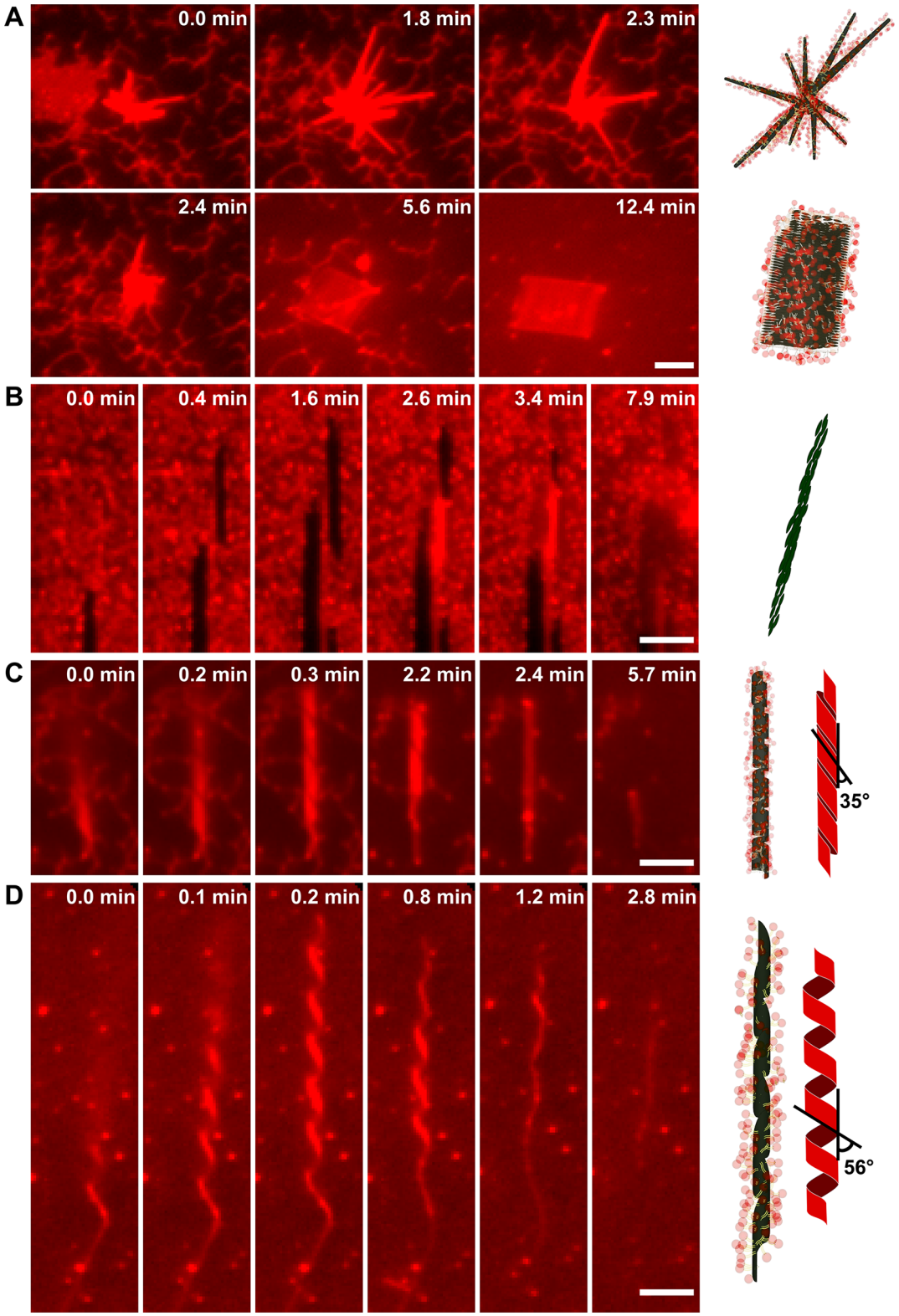

Figure 3. Microscopic observation of the dynamic cholesterol crystal evolution of metastable intermediates. Time-lapse micrographs of the dynamic cholesterol crystal growth from cholesterol-rich bicellar mixtures. The observation of (A) bundle of filament crystals transforming into crystal plate, (B) formation and disappearance of metastable rodlike crystals, and (C) low-pitch and (D) high-pitch helical crystals were captured *in situ*. The scale bars are 5 μm. The presented images are rotated for characterization, and the corresponding original micrographs and videos are provided in the Supporting Information.

1.5] due to Rh-PE, supporting the notion that the rod phase emerges from the interconversion of the initial fibrillar phase during this regime of structural evolution.

Concomitant to the formation of rods, two additional changes are evident: (1) the surface becomes more uniformly fluorescent, and rods acquire striking ballistic-like [trajectory

https://dx.doi.org/10.1021/jacs.0c10674
J. Am. Chem. Soc. XXXX, XXX, XXX−XXX

(μm)/time (s) = 0.14 μm/s] mobilities, seemingly gliding over the bilayer surface as consolidated "rafts" and conspicuously avoiding the growing cholesterol crystals devoid of fluorescence.[30,41] Together, these observations suggest gross molecular redistribution of lipids into a contiguous lipid bilayer and the formation of a three-dimensional, albeit lipid-covered, rod-shaped cholesterol crystal. These anisotropic elongated crystal morphologies do not represent morphological forms generally adopted by the triclinic habit of cholesterol monohydrate. They, however, resemble the initial assembly of cholesterol into filamentous crystals covered by amphiphilic lipids.

Similar filamentous intermediates have been previously reported to appear in dilute bile, and model bile suspensions containing high concentrations of cholesterol[42,43] were thought to represent the crystals either of the anhydrous or of the monohydrate states of cholesterol. More recently, however, similar rodlike morphologies of cholesterol crystals have also been observed in cholesterol−phospholipid mixtures and in intracellular locations of macrophages and resolved to represent the metastable monoclinic polymorph.[30] This early appearance of metastable cholesterol crystals from an initially unstable phase containing supersaturating cholesterol concentration in a lipid bilayer offers an early hint that cholesterol crystallization from a membrane phase might be governed by Ostwald's rule of stages.

Next, we observe that the rods, like their fibrillar precursors, also have limited lifetimes: some dissolve into growing rounded patches at the membrane surface (Figure 2A and Movie S2), whereas others evolve toward the equilibrium triclinic polymorph, some depleted in lipids (Figure 2B and Movie S3) and others covered by lipids (Figure 2C and Movie S4). The former is consistent with the dissolution of cholesterol from the rod phase into the membrane producing cholesterol-enriched domains reminiscent of lipid rafts.[44] At first, the cholesterol-rich patch appeared to be devoid of fluorophores, but over time (~15 min), the domains are seen to accumulate fluorophores as indicated by the increase of fluorescence intensity. The FRAP analysis performed in these domains shows slow and incomplete recovery, consistent with the elevated levels of cholesterol in these domains, which reduces the membrane fluidity by ordering the neighboring lipid acyl chains (Figure S2).[45]

The sequence of images shown in Figure 2B and Movie S3 provide an unambiguous example of the latter case in which rods convert into quadrilateral plates. Here, a mobile rod phase loses its translational mobility, abruptly loses fluorescence, and gradually widens to ultimately assume the quadrilateral geometry of a triclinic polymorph. The sequence of images also show that the triclinic polymorph does not grow from the aggregation of metastable rods but rather an isolated rod accrues the residual "free" cholesterol from the surrounding membrane and evolves into the triclinic habit. This metastable-to-stable transformation is fully irreversible, producing long-lived quadrilateral plates of cholesterol crystals.

Although this temporal evolution of cholesterol crystallization, characterized by the sequential appearance of fibrillar, rod-shaped, and quadrilateral plates, is fully reproducible in independent experiments, the morphological trajectory in different experiments reveals additional features. In some cases, the cluster of meshlike filament structure evolves into a lipid-bound stable plate crystal (Figure 3A and Movie S5) whereas the thin rodlike structure disappears after several minutes (~8 min) (Figure 3B and Movie S6). This suggests the transient nature of these morphologies.

Quite intriguingly, we often observe distinct helical ribbons (Figure S3 and Movies S7 and S8). Their lifetimes are short (<5 min) and emerge from the rod or fibril phase precursors (Figures 3C,D). Their structures reveal two different pitch angles: ~ 35° and ~56°. Comparable helical habits of cholesterol crystals, exhibiting high pitch (54°) and low-pitch (11°) conformations, were first reported in a model bile system containing a bile salt, a phospholipid, and cholesterol[42,46] and ascribed to be a metastable intermediate during crystallization of cholesterol leading to gallstone formation.[42] Subsequently, these cholesterol conformers, including an additional intermediate-pitch (~30°) variety, have also been observed to form in a variety of sterol-containing amphiphilic mixtures, including surfactants, lipids, and fatty acids.[47] Consistent with these findings, we also find that the helical polymorphs are short-lived, nucleate independently, and do not interconvert between each other.

Taken together, these observations of the sequential appearance and disappearance of fibrils, rods, and helices prior to the formation of rectangular plates of triclinic cholesterol monohydrate strongly suggest that, in addition to being influenced by different lipid environments,[30] the structurally distinct polymorphs of cholesterol are related to one another by Ostwald's rule of stages. The sequence of transformations beginning with lipid-coated fibrils and filaments, helices, rods, and quadrilateral plates suggests an early dimensional transition from 2D to 3D. It is consistent with the expected free energy steps from an initial unstable state based on Ostwald's criterion of the smallest drops in free energy compared to their immediate precursors.[42,43]

This spontaneous multistage crystallization of cholesterol from the bilayer environment ultimately creates two coexisting phases in equilibrium: the bilayer phase and the crystal phase. In this regime of phase coexistence, the chemical potential of cholesterol within the bilayer must be equal to that of the monohydrate crystal.[48] This then raises an interesting possibility: Can we catalyze the transfer of cholesterol between the two coexisting phases to further grow the extant cholesterol crystal? One of the best-known tools to effect cholesterol transport is a class of molecules called cyclodextrin (CD).[49] They are truncated-cone-shaped molecules consisting of discrete numbers of glucose units (αCD, 6; βCD, 7; and γCD, 8 glucose units) possessing a polar exterior and a hydrophobic central cavity. The polar exterior renders them water-soluble, and the hydrophobic cavity forms inclusion complexes with small hydrophobic substrates (guests). Among them, βCD presenting the central cavity of 7.8 Å ideally complexes with cholesterol and thus can serve as an efficient catalyst for extracting cholesterol from (and delivering to) the membranes.

To determine whether CDs can shift the equilibrium cholesterol distribution between the membrane and the monohydrate crystal, we first performed QCM-D experiments (Figure 4A). As described earlier, we use bicellar precursors to prepare supported lipid bilayers containing supersaturating concentration of cholesterol. The steady-state resonance frequency (Δf) and energy dissipation (ΔD) shifts are 72.4 ± 6.1 Hz and (10.1 ± 1.1) × 10^{-6} (n = 20), respectively. The two profiles follow the three sequential steps, including adsorption, fusion, and rupture, as described earlier. Subsequent incubation of these unstable supported bilayers with

https://dx.doi.org/10.1021/jacs.0c10674
J. Am. Chem. Soc. XXXX, XXX, XXX−XXX

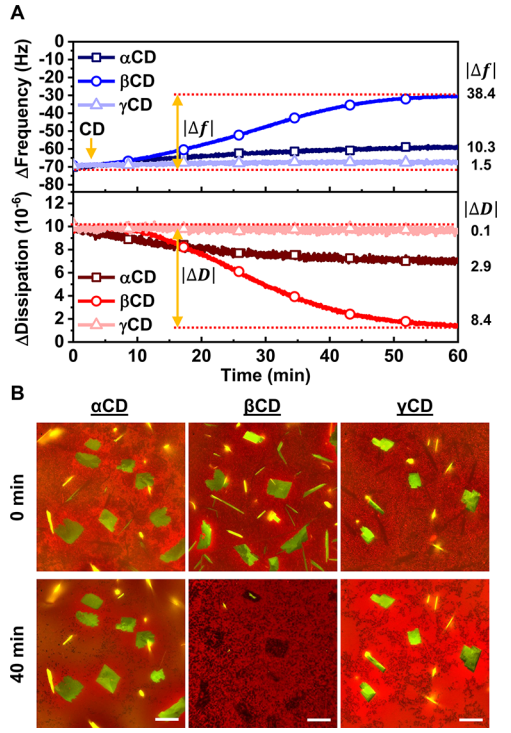

Figure 4. Time-resolved tracking of the interaction between native cyclodextrins (CDs) and cholesterol-enriched SLBs observed via QCM-D and fluorescence microscopy. (A) QCM-D measurements were performed to characterize the effect of CD treatments on mass and viscoelastic properties of cholesterol-rich SLBs. The initial measurement values correspond to fabricated SLBs after a buffer rinsing step, and 1 mM CD was added at t = 3 min. (B) Time-lapse fluorescence microscopy images show the effect of CDs on the cholesterol crystals (BODIPY-cholesterol, green) and cholesterol-rich lipid membranes (Rh-PE, red). The red and green channels are merged and presented together. The native CDs were injected at t = 0 min, and the scale bars are 20 μm.

βCDs (1 mM, t = 3 min) triggered a large response characterized by the net Δf and ΔD shifts of 38.4 Hz and 8.4 × 10^{-6}, respectively. By comparison, the αCD and γCD triggered only a marginal response.

To investigate the morphological changes caused by the action of CDs, we next conducted time-lapse fluorescence microscopy imaging experiments (Figure S4). To enable simultaneous visualization of the crystal and the membrane phases, we doped the cholesterol fraction using fluorescent boron−dipyrromethene (BODIPY)−cholesterol (0.5 mol % with respect to cholesterol)[50,51] and stained the membrane phase using Rh-PE. The use of trace concentrations of fluorescently labeled cholesterol did not qualitatively change the multistage crystallization (see above) pathway, although we observed larger and more numerous crystal plates and rod-shaped crystals. Upon incubation of the supported bilayers with 1 mM CDs in a constant flow for 40 min, distinct effects were evaluated (Figure 4B, Figure S5, and Movies S9−S11). βCD induced (1) near-complete removal of cholesterol crystals and (2) the appearance of a large number of holes dispersed throughout the membrane phase. This then provides an early indication that βCD is effective in removing cholesterol from both the crystal and the membrane phase.[52,53] In addition, respective bicellar mixtures composed of unlabeled lipids, single labeled lipids (only Rh-PE), and double-labeled lipids (Rh-PE and BODIPY-cholesterol) were tested to confirm the formation and removal of cholesterol crystals induced by βCD via QCM-D measurements (Figure S6). The overall kinetics and maximum/minimum peaks of frequency/dissipation shifts were similar in all three cases, which supports the consistency of the platform regardless of dye inclusions. Furthermore, monitoring of fluorescence images during βCD and single-labeled membrane also revealed that βCD can extract cholesterol crystals within 30 min, leaving the traces of defects with significant alterations in the membranes (Figure S7).

A closer examination of the dynamics of cholesterol removal, however, suggests a more nuanced picture as revealed by the time-lapsed fluorescence microscopy images, together with surface plots (Figure 5). Curiously, within minutes (∼3 min) after αCD injection, the fluorescence intensity of the top right corner of the crystal began to exhibit a surprising increase, suggesting cholesterol accumulation rather than depletion. Similar unexpected behavior followed in other regions of the same crystal plate a little later (∼9 min) (Figure 5A). This unusual behavior is best illustrated by the quantitative surface plots of BODIPY-cholesterol intensity in Figure 5B. Qualitatively similar trends are seen for both βCD and γCD. These observations suggest that all three cyclodextrins, albeit with different kinetics and with varied efficiencies, catalyze the transfer of cholesterol between the two, membrane and the crystal, phases. Specifically, they extract cholesterol from the membrane phase and deliver to the crystal phase, thereby growing the crystal layer-by-layer before effecting the dissolution of the crystal itself.

CONCLUSION

The findings reported here are significant in three distinct regards. First, by enabling the preparation of supported bilayers supersaturated with cholesterol, bicellar precursors allow real-time monitoring of the morphological evolution and dynamics that attend cholesterol crystallization. The approach is versatile and can be readily extended—beyond cholesterol crystallization—to other membrane components and phenomena, such as crystallization of transmembrane proteins occurring during overexpression and liquid−liquid phase separation, which ensues due to abnormal trafficking of lipids to membranes. Second, our findings confirm that the three-dimensional crystallization of cholesterol from the membrane phase follows a multistage route, producing a variety of crystalline polymorphs en route to the formation of the thermodynamically most stable quadrilateral plates, consistent with the predictions of Ostwald's rule of stages. This then suggests that the appearance of transient intermediates is not merely a consequence of local lipid microenvironment but rather a requisite step preceding the formation of the equilibrium phase of cholesterol monohydrates. Third, the ability of cyclodextrin to catalyze the transfer of cholesterol between the membrane and the crystal phase and ensuing layer-by-layer growth of cholesterol crystals further suggests how additional cholesterol—either exogenously supplanted or catalytically trafficked—might become incorporated into existing crystals.

EXPERIMENTAL SECTION

Reagents. 1,2-Dioleoyl-*sn*-glycero-3-phosphocholine (DOPC), 1,2-dihexanoyl-*sn*-glycero-3-phosphocholine (DHPC), 1,2-dioleoyl-*sn*-glycero-3-phosphoethanolamine-*N*-(lissamine rhodamine B sulfonyl) (ammonium salt) (red, Rh-PE) and 23-(dipyrromethene boron

https://dx.doi.org/10.1021/jacs.0c10674
J. Am. Chem. Soc. XXXX, XXX, XXX−XXX

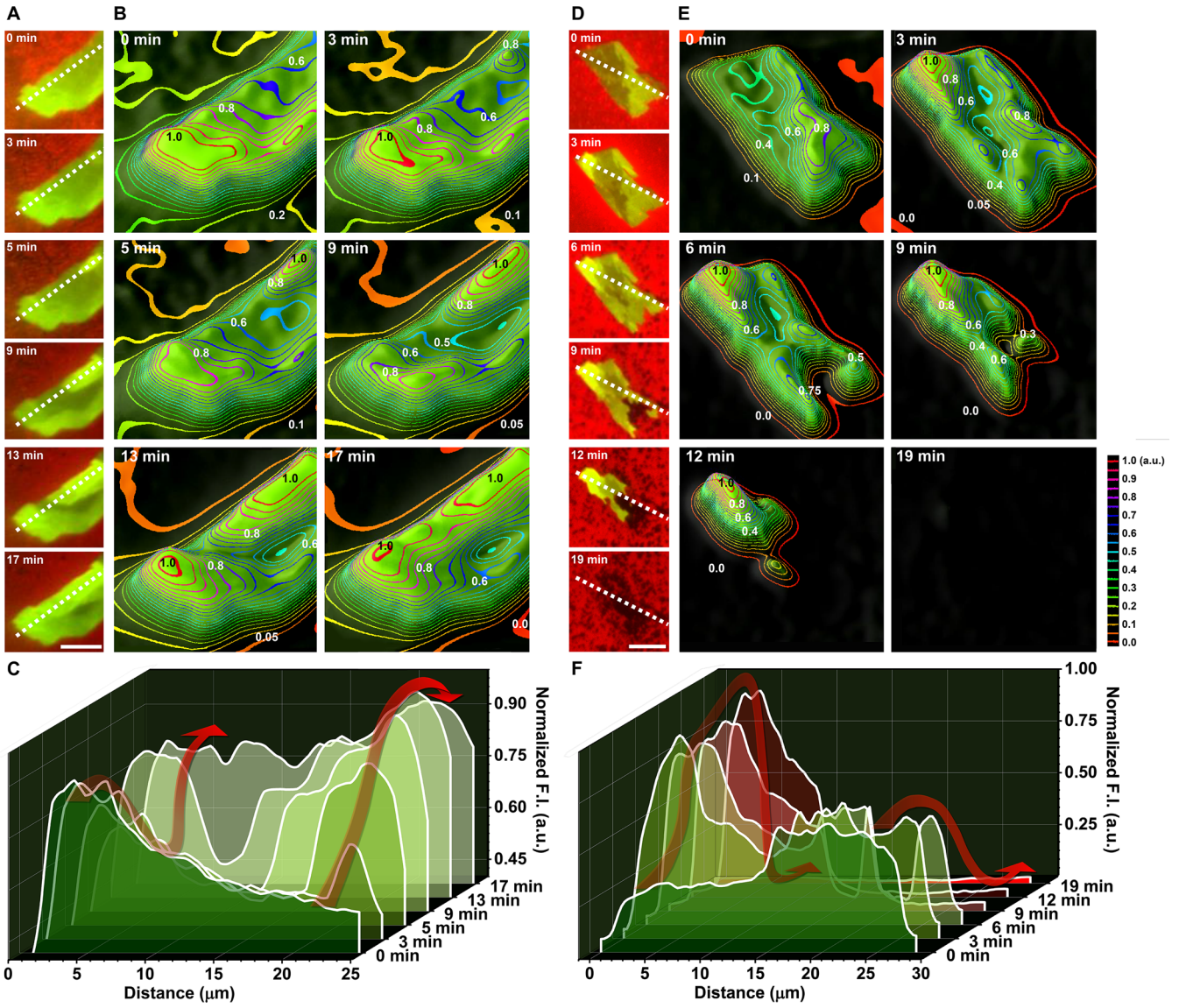

Figure 5. Fluorescence intensity analysis of single crystals induced by αCD and βCD. (A) Time-lapsed fluorescence microscopy images of fluorescently labeled phospholipid (Rh-PE, red) and cholesterol (BODIPY-cholesterol, green) on a surface. 1 mM αCD was added at t = 0 min. (B) Surface plot of the time-resolved fluorescence intensity (F.I.) of a single crystal from data in a (green). The contour lines connect the area with relatively similar F.I., and the intensity values were normalized by maximum and minimum values as 1.0 and 0.0 au, respectively. (C) Line fluorescence intensity (F.I.) profile from data in a (white dotted line). (D−F) Corresponding data obtained from the treatment of βCD. The scale bars are 10 μm (note the different scales).

difluoride)-24-norcholesterol (green, BODIPY-cholesterol or BODIPY-Chol) lipids dissolved in chloroform, and cholesterol powder were obtained from Avanti Polar Lipids (Alabaster, AL). The excitation/emission wavelengths of Rh-PE and BODIPY-Chol are 560/583 nm and 495/507 nm, respectively. Cyclodextrins (CDs) including αCD, βCD, and γCD were purchased from CycloLab (Budapest, Hungary). The buffer used in all experiments was 10 mM Tris buffer with 150 mM NaCl (pH 7.5). Buffers and solutions were prepared with Milli-Q-treated water (MilliporeSigma, Burlington, MA).

Bicellar Mixture Preparation. First, the appropriate amounts of long-chain DOPC, cholesterol lipids, and short-chain DHPC lipids in chloroform were added to a glass vial, and then the solvent was evaporated by nitrogen gas, forming a dry lipid film. For the fluorescence microscopy experiments, 0.5 mol % Rh-PE and/or 0.5 mol % of BODIPY-Chol was included with respect to the amount of DOPC and/or cholesterol, respectively. For instance, the long-chain lipid composition of 80 mol % cholesterol bicellar mixtures with both dyes included 19.9, 0.1, 79.6, and 0.4 mol % of DOPC, Rh-PE, cholesterol, and BODIPY-cholesterol, respectively. After overnight storage in a vacuum desiccator, the dried lipid film was hydrated in aqueous buffer solution (10 mM Tris with 150 mM NaCl, pH 7.5) to a q ratio of 0.25 (i.e., 1 mM long-chain lipids/4 mM DHPC). The lipid suspension was then subjected to five freeze−thaw−vortex cycles, involving the following steps: (1) submerse in liquid nitrogen for 1 min, (2) thaw in a 60 °C water bath for 5 min, and (3) vortex for 30 s. Immediately before the experiment, an aliquot of the stock lipid suspension was diluted 32-fold by using the buffer solution. Therefore, the final long- and short-chain lipid concentrations used in the experiments were 0.031 and 0.125 mM, respectively.

Dynamic Light Scattering (DLS). The corresponding measurements were performed on a 90Plus particle size analyzer (Brookhaven Instruments Corporation, New York) at a scattering angle of 90° where the reflection effect is minimized. All autocorrelation functions obtained were analyzed by the cumulants method and fitted to log-normal distribution(s) to obtain the size distribution. The bicellar mixtures showed three distinct peaks around 50, 1000, and >2000 nm (Figure S8). The larger and broader diameter compared to conventional bicelles (100% DOPC ranges 20−50 nm) implies that

https://dx.doi.org/10.1021/jacs.0c10674
J. Am. Chem. Soc. XXXX, XXX, XXX−XXX

there are cholesterol−phospholipid aggregates that can be further characterized.

Quartz Crystal Microbalance−Dissipation (QCM-D). The QCM-D experiments were conducted by using a Q-Sense E4 instrument (Biolin Scientific AB, Stockholm, Sweden). The quartz crystal sensors were repeatedly rinsed with 1% (w/v) sodium lauryl sulfate (SDS) solution, deionized water, and 95% ethanol, dried with nitrogen gas, and then treated in an oxygen plasma chamber (PDC-002, Harrick Plasma, Ithaca, NY) for 1 min. The temperature of the QCM-D chambers was maintained at 25 °C. All solutions were added under continuous flow conditions by using a peristaltic pump (Reglo Digital, Ismatec, Glattbrugg, Switzerland), and the flow rate was set at 100 μL/min. Measurement data were collected at multiple odd overtones by the Q-Soft software package (Biolin Scientific AB). The reported data were collected at the seventh overtone and normalized according to the overtone number. Data processing was completed by using the Q-Tools (Biolin Scientific AB) and OriginPro (OriginLab, Northampton, MA) software programs.

Epifluorescence Microscopy. Imaging experiments were conducted by using a Nikon Eclipse Ti-E inverted microscope with a 60× oil-immersion objective (NA 1.49). The excitation source was a mercury-fiber illuminator C-HGFIE Intensilight (Nikon, Tokyo, Japan), and the light was passed through an alternating dichroic filter block (Ex 480/40, Em 535/50) or (Ex 545/30, Em 605/70) for imaging in the green and red channels, respectively. An Andor iXon3 897 EMCCD camera was used to obtain the images at the rate of 1 frame per 3 s. Glass coverslips (ibidi GmbH, Martinsried, Germany) were subsequently rinsed with 1% (w/v) SDS solution, deionized water, and 95% ethanol. Then the substrate was dried with nitrogen gas and treated with oxygen plasma (model no. PDC-002, Harrick Plasma, Ithaca, NY) for 1 min to render the surface hydrophilic before being assembled in a microfluidic chamber (sticky-Slide VI 0.4, ibidi GmbH, Martinsried, Germany). The liquid sample was introduced at a flow rate of 100 μL/min, as controlled by a peristaltic pump (model no. ISM833C, Ismatec, Wertheim, Germany). All measurements were conducted at room temperature (~25 °C).

Fluorescence Recovery after Photobleaching (FRAP). The lateral diffusivity of fluorescently labeled Rh-PE lipids within an SLB was measured by the fluorescence recovery after the photobleaching (FRAP) technique.[31] For fluorescence recovery after photobleaching (FRAP) analysis, a single-mode laser source of 532 nm (100 mW, Coherent Inc., Santa Clara, CA) was used to photobleach a circular spot of 20 μm in diameter within the fabricated lipid membranes. Subsequently, fluorescence micrographs were captured for 2−6 min at 2 s intervals to track the fluorescence recovery. For the clear bilayer domain, the diffusivity was measured by the Hankel transform method.[32] The measurement was independently repeated five times in total.

■ ASSOCIATED CONTENT

Supporting Information

The Supporting Information is available free of charge at https://pubs.acs.org/doi/10.1021/jacs.0c10674.

Additional information including bright-field and fluorescence microscopy (Figure S1), fluorescence recovery after photobleaching (FRAP) observation (Figure S2), the original time-lapse micrographs (Figure S3), the observation of the supported lipid membrane formation with double dyes (Figure S4), time-resolved tracking of CD interaction in full view (Figure S5), comparison of dye inclusions (Figure S6), micrographs showing the effect of βCD on Rh-PE membrane (Figure S7), and dynamic light scattering (DLS) measurements (Figure S8) (PDF)

Movies S1−S11 (ZIP)

■ AUTHOR INFORMATION

Corresponding Author

Nam-Joon Cho − *School of Materials Science and Engineering, Nanyang Technological University, 639798 Singapore, Singapore; Department of Biomedical Engineering, University of California, Davis, Davis, California 95616, United States;* orcid.org/0000-0002-8692-8955; Email: njcho@ntu.edu.sg

Authors

Soohyun Park − *School of Materials Science and Engineering, Nanyang Technological University, 639798 Singapore, Singapore;* orcid.org/0000-0003-3261-7585

Tun Naw Sut − *School of Materials Science and Engineering, Nanyang Technological University, 639798 Singapore, Singapore*

Gamaliel Junren Ma − *School of Materials Science and Engineering, Nanyang Technological University, 639798 Singapore, Singapore;* orcid.org/0000-0002-6740-1031

Atul N. Parikh − *School of Materials Science and Engineering, Nanyang Technological University, 639798 Singapore, Singapore; Department of Biomedical Engineering, University of California, Davis, Davis, California 95616, United States;* orcid.org/0000-0002-5927-4968

Complete contact information is available at: https://pubs.acs.org/10.1021/jacs.0c10674

Notes

The authors declare no competing financial interest.

■ ACKNOWLEDGMENTS

The authors thank Dr. Jay T. Groves for stimulating discussions. This work was supported by the National Research Foundation of Singapore through a Competitive Research Programme Grant (NRF-CRP10-2012-07) and a Proof-of-Concept Grant (NRF2015NRF-POC0001-19).

■ REFERENCES

(1) Onuki, A. *Phase Transition Dynamics*; Cambridge University Press: Cambridge, 2002.

(2) Bray, A. J. Theory of Phase-Ordering Kinetics. *Adv. Phys.* **1994**, *43* (3), 357−459.

(3) Ostwald, W. Studien über die Bildung und Umwandlung fester Körper. *Z. Phys. Chem.* **1897**, *22* (1), 289−330.

(4) tenWolde, P. R.; Frenkel, D. Enhancement of Protein Crystal Nucleation by Critical Density Fluctuations. *Science* **1997**, *277* (5334), 1975−1978.

(5) Anderson, V. J.; Lekkerkerker, H. N. W. Insights into Phase Transition Kinetics from Colloid Science. *Nature* **2002**, *416* (6883), 811−815.

(6) Gasser, U.; Weeks, E. R.; Schofield, A.; Pusey, P. N.; Weitz, D. A. Real-Space Imaging of Nucleation and Growth in Colloidal Crystallization. *Science* **2001**, *292* (5515), 258−262.

(7) Nielsen, M. H.; Aloni, S.; De Yoreo, J. J. In Situ TEM Imaging of CaCO3 Nucleation Reveals Coexistence of Direct and Indirect Pathways. *Science* **2014**, *345* (6201), 1158−1162.

(8) Shoemaker, D. P.; Hu, Y. J.; Chung, D. Y.; Halder, G. J.; Chupas, P. J.; Soderholm, L.; Mitchell, J. F.; Kanatzidis, M. G. In Situ Studies of a Platform for Metastable Inorganic Crystal Growth and Materials Discovery. *Proc. Natl. Acad. Sci. U. S. A.* **2014**, *111* (30), 10922−10927.

(9) Stein, A.; Keller, S. W.; Mallouk, T. E. Turning down the Heat - Design and Mechanism in Solid-State Synthesis. *Science* **1993**, *259* (5101), 1558−1564.

(10) Simons, K.; Sampaio, J. L. Membrane Organization and Lipid Rafts. *Cold Spring Harbor Perspect. Biol.* **2011**, *3* (10), 17.
(11) Vereb, G.; Szollosi, J.; Matko, J.; Nagy, P.; Farkas, T.; Vigh, L.; Matyus, L.; Waldmann, T. A.; Damjanovich, S. Dynamic, Yet Structured: The Cell Membrane Three Decades after the Singer-Nicolson Model. *Proc. Natl. Acad. Sci. U. S. A.* **2003**, *100* (14), 8053−8058.
(12) Bach, D.; Wachtel, E. Phospholipid/Cholesterol Model Membranes: Formation of Cholesterol Crystallites. *Biochim. Biophys. Acta, Biomembr.* **2003**, *1610* (2), 187−197.
(13) Landau, E. M.; Rosenbusch, J. P. Lipidic Cubic Phases: A Novel Concept for the Crystallization of Membrane Proteins. *Proc. Natl. Acad. Sci. U. S. A.* **1996**, *93* (25), 14532−14535.
(14) Chung, S.; Shin, S. H.; Bertozzi, C. R.; De Yoreo, J. J. Self-Catalyzed Growth of S Layers via an Amorphous-to-Crystalline Transition Limited by Folding Kinetics. *Proc. Natl. Acad. Sci. U. S. A.* **2010**, *107* (38), 16536−16541.
(15) Shin, S. H.; Chung, S.; Sanii, B.; Comolli, L. R.; Bertozzi, C. R.; De Yoreo, J. J. Direct Observation of Kinetic Traps Associated with Structural Transformations Leading to Multiple Pathways of S-Layer Assembly. *Proc. Natl. Acad. Sci. U. S. A.* **2012**, *109* (32), 12968−12973.
(16) Yang, L.; Weiss, T. M.; Lehrer, R. I.; Huang, H. W. Crystallization of Antimicrobial Pores in Membranes: Magainin and Protegrin. *Biophys. J.* **2000**, *79* (4), 2002−2009.
(17) Huang, J. Y.; Buboltz, J. T.; Feigenson, G. W. Maximum Solubility of Cholesterol in Phosphatidylcholine and Phosphatidylethanolamine Bilayers. *Biochim. Biophys. Acta, Biomembr.* **1999**, *1417* (1), 89−100.
(18) Duewell, P.; Kono, H.; Rayner, K. J.; Sirois, C. M.; Vladimer, G.; Bauernfeind, F. G.; Abela, G. S.; Franchi, L.; Nuñez, G.; Schnurr, M.; et al. NLRP3 Inflammasomes are Required for Atherogenesis and Activated by Cholesterol Crystals. *Nature* **2010**, *464* (7293), 1357−1361.
(19) Rajamäki, K.; Lappalainen, J.; Öörni, K.; Välimäki, E.; Matikainen, S.; Kovanen, P. T.; Eklund, K. K. Cholesterol Crystals Activate the NLRP3 Inflammasome in Human Macrophages: A Novel Link Between Cholesterol Metabolism and Inflammation. *PLoS One* **2010**, *5* (7), e11765.
(20) Admirand, W. H.; Small, D. M. The Physicochemical Basis of Cholesterol Gallstone Formation in Man. *J. Clin. Invest.* **1968**, *47* (5), 1043−1052.
(21) Sedaghat, A.; Grundy, S. M. Cholesterol Crystals and the Formation of Cholesterol Gallstones. *N. Engl. J. Med.* **1980**, *302* (23), 1274−1277.
(22) Pang, C. E.; Messinger, J. D.; Zanzottera, E. C.; Freund, K. B.; Curcio, C. A. The Onion Sign in Neovascular Age-Related Macular Degeneration Represents Cholesterol Crystals. *Ophthalmology* **2015**, *122* (11), 2316−2326.
(23) Ziblat, R.; Kjaer, K.; Leiserowitz, L.; Addadi, L. Structure of Cholesterol/Lipid Ordered Domains in Monolayers and Single Hydrated Bilayers. *Angew. Chem., Int. Ed.* **2009**, *48* (47), 8958−8961.
(24) Ziblat, R.; Leiserowitz, L.; Addadi, L. Crystalline Domain Structure and Cholesterol Crystal Nucleation in Single Hydrated DPPC:Cholesterol:POPC Bilayers. *J. Am. Chem. Soc.* **2010**, *132* (28), 9920−9927.
(25) Ziblat, R.; Leiserowitz, L.; Addadi, L. Crystalline Lipid Domains: Characterization by X-Ray Diffraction and their Relation to Biology. *Angew. Chem., Int. Ed.* **2011**, *50* (16), 3620−3629.
(26) Ziblat, R.; Fargion, I.; Leiserowitz, L.; Addadi, L. Spontaneous formation of two-dimensional and three-dimensional cholesterol crystals in single hydrated lipid bilayers. *Biophys. J.* **2012**, *103* (2), 255−264.
(27) Solomonov, I.; Weygand, M. J.; Kjaer, K.; Rapaport, H.; Leiserowitz, L. Trapping Crystal Nucleation of Cholesterol Monohydrate: Relevance to Pathological Crystallization. *Biophys. J.* **2005**, *88* (3), 1809−1817.
(28) Varsano, N.; Fargion, I.; Wolf, S. G.; Leiserowitz, L.; Addadi, L. Formation of 3D cholesterol crystals from 2D nucleation sites in lipid bilayer membranes: implications for atherosclerosis. *J. Am. Chem. Soc.* **2015**, *137* (4), 1601−1607.
(29) Varsano, N.; Beghi, F.; Dadosh, T.; Elad, N.; Pereiro, E.; Haran, G.; Leiserowitz, L.; Addadi, L. The Effect of the Phospholipid Bilayer Environment on Cholesterol Crystal Polymorphism. *ChemPlusChem.* **2019**, *84* (4), 338−344.
(30) Varsano, N.; Beghi, F.; Elad, N.; Pereiro, E.; Dadosh, T.; Pinkas, I.; Perez-Berna, A. J.; Jin, X. T.; Kruth, H. S.; Leiserowitz, L.; Addadi, L. Two Polymorphic Cholesterol Monohydrate Crystal Structures form in Macrophage Culture Models of Atherosclerosis. *Proc. Natl. Acad. Sci. U. S. A.* **2018**, *115* (30), 7662−7669.
(31) Carnell, M.; Macmillan, A.; Whan, R. Fluorescence Recovery after Photobleaching (FRAP): Acquisition, Analysis, and Applications. In *Methods in Membrane Lipids*; Springer: 2015; pp 255−271.
(32) Jönsson, P.; Jonsson, M. P.; Tegenfeldt, J. O.; Höök, F. A Method Improving the Accuracy of Fluorescence Recovery after Photobleaching Analysis. *Biophys. J.* **2008**, *95* (11), 5334−5348.
(33) Sut, T. N.; Park, S.; Choe, Y.; Cho, N.-J. Characterizing the Supported Lipid Membrane Formation from Cholesterol-Rich Bicelles. *Langmuir* **2019**, *35* (47), 15063−15070.
(34) Kolahdouzan, K.; Jackman, J. A.; Yoon, B. K.; Kim, M. C.; Johal, M. S.; Cho, N.-J. Optimizing the Formation of Supported Lipid Bilayers from Bicellar Mixtures. *Langmuir* **2017**, *33* (20), 5052−5064.
(35) Sut, T. N.; Jackman, J. A.; Yoon, B. K.; Park, S.; Kolahdouzan, K.; Ma, G. J.; Zhdanov, V. P.; Cho, N.-J. Influence of NaCl Concentration on Bicelle-Mediated SLB Formation. *Langmuir* **2019**, *35* (32), 10658−10666.
(36) Jackman, J. A.; Cho, N.-J. Supported Lipid Bilayer Formation: Beyond Vesicle Fusion. *Langmuir* **2020**, *36* (6), 1387−1400.
(37) Pomorska, A.; Shchukin, D.; Hammond, R.; Cooper, M. A.; Grundmeier, G.; Johannsmann, D. Positive Frequency Observed upon Adsorbing Micron-Sized Solid Objects to a Quartz Crystal Microbalance from the Liquid Phase. *Anal. Chem.* **2010**, *82* (6), 2237−2242.
(38) Granéli, A.; Edvardsson, M.; Höök, F. DNA-Based Formation of a Supported, Three-Dimensional Lipid Vesicle Matrix Probed by QCM-D and SPR. *ChemPhysChem* **2004**, *5* (5), 729−733.
(39) Dunér, G.; Thormann, E.; Dėdinaitė, A. Quartz Crystal Microbalance with Dissipation (QCM-D) studies of the viscoelastic response from a continuously growing grafted polyelectrolyte layer. *J. Colloid Interface Sci.* **2013**, *408*, 229−234.
(40) Lapidot, T.; Sedransk Campbell, K. L.; Heng, J. Y. Model for Interpreting Surface Crystallization Using Quartz Crystal Microbalance: Theory and Experiments. *Anal. Chem.* **2016**, *88* (9), 4886−4893.
(41) Craven, B. M. Crystal Structure of Cholesterol Monohydrate. *Nature* **1976**, *260* (5553), 727−729.
(42) Konikoff, F.; Chung, D.; Donovan, J.; Small, D.; Carey, M. Filamentous, Helical, and Tubular Microstructures During Cholesterol Crystallization from Bile. Evidence that Cholesterol Does not Nucleate Classic Monohydrate Plates. *J. Clin. Invest.* **1992**, *90* (3), 1155−1160.
(43) Konikoff, F. M.; Cohen, D. E.; Carey, M. C. Filamentous Crystallization of Cholesterol and its Dependence on Lecithin Species in Bile. *Mol. Cryst. Liq. Cryst. Sci. Technol., Sect. A* **1994**, *248* (1), 291−296.
(44) Crane, J. M.; Tamm, L. K. Role of Cholesterol in the Formation and Nature of Lipid Rafts in Planar and Spherical Model Membranes. *Biophys. J.* **2004**, *86* (5), 2965−2979.
(45) Yang, S.-T.; Kreutzberger, A. J.; Lee, J.; Kiessling, V.; Tamm, L. K. The Role of Cholesterol in Membrane Fusion. *Chem. Phys. Lipids* **2016**, *199*, 136−143.
(46) Chung, D. S.; Benedek, G. B.; Konikoff, F. M.; Donovan, J. M. Elastic Free Energy of Anisotropic Helical Ribbons as Metastable Intermediates in the Crystallization of Cholesterol. *Proc. Natl. Acad. Sci. U. S. A.* **1993**, *90* (23), 11341−11345.
(47) Zastavker, Y. V.; Asherie, N.; Lomakin, A.; Pande, J.; Donovan, J. M.; Schnur, J. M.; Benedek, G. B. Self-Assembly of Helical Ribbons. *Proc. Natl. Acad. Sci. U. S. A.* **1999**, *96* (14), 7883−7887.

https://dx.doi.org/10.1021/jacs.0c10674
J. Am. Chem. Soc. XXXX, XXX, XXX−XXX

(48) Huang, J. Y.; Feigenson, G. W. A Microscopic Interaction Model of Maximum Solubility of Cholesterol in Lipid Bilayers. *Biophys. J.* **1999**, *76* (4), 2142−2157.
(49) Kilsdonk, E. P. C.; Yancey, P. G.; Stoudt, G. W.; Bangerter, F. W.; Johnson, W. J.; Phillips, M. C.; Rothblat, G. H. Cellular Cholesterol Efflux Mediated by Cyclodextrins. *J. Biol. Chem.* **1995**, *270* (29), 17250−17256.
(50) Ariola, F. S.; Li, Z.; Cornejo, C.; Bittman, R.; Heikal, A. A. Membrane Fluidity and Lipid Order in Ternary Giant Unilamellar Vesicles Using a New Bodipy-Cholesterol Derivative. *Biophys. J.* **2009**, *96* (7), 2696−2708.
(51) Marks, D. L.; Bittman, R.; Pagano, R. E. Use of Bodipy-Labeled Sphingolipid and Cholesterol Analogs to Examine Membrane Microdomains in Cells. *Histochem. Cell Biol.* **2008**, *130* (5), 819.
(52) Zimmer, S.; Grebe, A.; Bakke, S. S.; Bode, N.; Halvorsen, B.; Ulas, T.; Skjelland, M.; De Nardo, D.; Labzin, L. I.; Kerksiek, A.; et al. Cyclodextrin Promotes Atherosclerosis Regression via Macrophage Reprogramming. *Sci. Transl. Med.* **2016**, *8* (333), 333ra50−333ra50.
(53) Zidovetzki, R.; Levitan, I. Use of Cyclodextrins to Manipulate Plasma Membrane Cholesterol Content: Evidence, Misconceptions and Control Strategies. *Biochim. Biophys. Acta, Biomembr.* **2007**, *1768* (6), 1311−1324.

https://dx.doi.org/10.1021/jacs.0c10674
J. Am. Chem. Soc. XXXX, XXX, XXX−XXX